

Liquid phase epitaxy magnetic garnet films and applications

Yi-Heng Rao(饶毅恒), Huai-Wu Zhang(张怀武), Qing-Hui Yang(杨青慧), Dai-Nan Zhang(张岱南), Li-Chuan Jin(金立川), Bo Ma(马博), Yu-Juan Wu(吴玉娟)

Citation: Chin. Phys. B . 2018, 27(8): 086701. **doi:** 10.1088/1674-1056/27/8/086701

Journal homepage: http://cpb.iphy.ac.cn; http://iopscience.iop.org/cpb

What follows is a list of articles you may be interested in

Optical properties of a three-dimensional chiral metamaterial

Juan-Juan Guo(郭娟娟), Mao-Sheng Wang(汪茂胜), Wan-Xia Huang(黄万霞)

Chin. Phys. B . 2017, 26(12): 124211. **doi:** 10.1088/1674-1056/26/12/124211

Optical properties of Mg^{2+}, Yb^{3+}, and Ho^{3+} tri-doped $LiNbO_3$ crystals

Li Dai(代丽), Chun-Rui Liu(刘春蕊), Chao Tan(谭超), Zhe-Hua Yan(阎哲华), Yu-Heng Xu(徐玉恒)

Chin. Phys. B . 2017, 26(4): 044207. **doi:** 10.1088/1674-1056/26/4/044207

Photoluminescence characteristics of ZnTe bulk crystal and ZnTe epilayer grown on GaAs substrate by MOVPE

Lü Hai-Yan, Mu Qi, Zhang Lei, Lü Yuan-Jie, Ji Zi-Wu, Feng Zhi-Hong, Xu Xian-Gang, Guo Qi-Xin

Chin. Phys. B . 2015, 24(12): 124207. **doi:** 10.1088/1674-1056/24/12/124207

Design and optimization of a SiC thermal emitter/absorber composed of periodic microstructures based on a non-linear method

Wang Wei-Jie, Zhao Zhen-Guo, Zhao Yi, Zhou Hai-Jing, Fu Ce-Ji

Chin. Phys. B . 2015, 24(9): 094213. **doi:** 10.1088/1674-1056/24/9/094213

\A cold ^{87}Rb atomic beam

Wang Xiao-Jia, Feng Yan-Ying, Xue Hong-Bo, Zhou Zhao-Ying, Zhang Wen-Dong

Chin. Phys. B . 2011, 20(12): 126701. **doi:** 10.1088/1674-1056/20/12/126701

REVIEW

Liquid phase epitaxy magnetic garnet films and their applications*

Yi-Heng Rao(饶毅恒)[1], Huai-Wu Zhang(张怀武)[1,†], Qing-Hui Yang(杨青慧)[1], Dai-Nan Zhang(张岱南)[1,2], Li-Chuan Jin(金立川)[1], Bo Ma(马博)[1], and Yu-Juan Wu(吴玉娟)[1]

[1] *University of Electronic Science and Technology of China, Chengdu* 610054, *China*
[2] *University of Delaware, Newark, DE* 19716, *USA*

(Received 24 February 2018; revised manuscript received 7 May 2018; published online 25 July 2018)

Liquid phase epitaxy (LPE) is a mature technology. Early experiments on single magnetic crystal films fabricated by LPE were focused mainly on thick films for microwave and magneto–optical devices. The LPE is an excellent way to make a thick film, low damping magnetic garnet film and high-quality magneto–optical material. Today, the principal challenge in the applied material is to create sub-micrometer devices by using modern photolithography technique. Until now the magnetic garnet films fabricated by LPE still show the best quality even on a nanoscale (about 100 nm), which was considered to be impossible for LPE method.

Keywords: liquid phase epitaxy (LPE), magnetic garnet, magneto–optical, spintronics, magnonics

PACS: 67.30.hj, 42.70.–a **DOI:** 10.1088/1674-1056/27/8/086701

1. Introduction

The liquid phase epitaxy (LPE) has been used in the production of silicon, germanium, SiC, and II–VI and IV–VI compound semiconductors, as well as magnetic garnets, superconductors, ferroelectrics, and other optical materials. The LPE can produce epitaxial layers of superior material quality, concerning minority carrier lifetime, low damping parameter and thick films. The growth rate of LPE is almost 10–100 times faster than that of molecular beam epitaxy (MBE), metal–organic chemical vapor deposition (MOCVD), radio frequency(RF)-sputtering and pulsed laser deposition (PLD), which is in a range of 0.1 μm/min–1 μm/min. Capper and Mark gave a conclusion of the advantages of LPE as follows.[1] This growth rate is preferable for device structures to need thick films. The wide range of dopants is available for garnet with various properties via LPE. Almost any element in the melt will be incorporated into the epitaxial layer to some certain degree. Most of the elements in the periodic table can be utilised as dopants in LPE, and thus, LPE is an excellent tool for fundamental doping studies. The LPE can produce material of extremely high purity. The low point defect densities are due to near-equilibrium growth conditions and favourable chemical potentials of crystal components in the liquid phase. Neither the highly toxic precursors nor the by-products are existent. Unlike the equipment PLD or MBE, the LPE has the low-cost equipment and operation except the platinum accessories, and also possesses the ability to produce shaped or faceted crystals for novel device structures.

In this review, we address the liquid phase epitaxy (LPE) equipment fabricated magnetic garnet films, which have been widely used in spintronics, magnonics, microwave devices, THz devices and magneto–optical devices. The microwave device, THz devices and magneto–optical devices require garnet films with the thickness ranging from a few microns to dozens of microns, which is feasible with LPE. However, the field of science that refers to information transport and processing by spin waves is known as magnonics, and the usage of magnonic approaches in the field of spintronics needs film thickness to decrease down to a nanoscale. This thickness range was considered to exceed the ability of LPE. Recent work has successfully grown a yttrium iron garnet film on a gadolinium gallium garnet and its thickness reaches to nanoscale (< 100 nm)[2] with a more perfect match between the substrate and LPE film than other methods (RF, MBE, PLD, CVD).[3]

In this paper, we address the main achievements in magnetic garnet fabricated by dipping method LPE in the last fifty years. Other LPE methods include Nelson method, sliding-boat method, and rotating-crucible method are not discussed in this paper. An attempt is made to cover the study of both spintronics/magnonics and magneto–optical applications and the development of the LPE equipment and technology.[1]

The rest of this paper is organized as follows. In Section 1 we give a short introduction of the technological advantages and performance of LPE equipment. This section is based

*Project supported by the National Key Research and Development Program of China (Grant No. 2016YFA0300801), the National Natural Science Foundation of China (Grant Nos. 51702042, 61734002, 61571079, 51572042, and 61471096), the International Science & Technology Cooperation Program of China (Grant No. 2015DFR50870), and the Sichuan Science and Technology Support Project, China (Grant Nos. 2016GZ0250 and 2017JY0002).

†Corresponding author. E-mail: hwzhang@uestc.edu.cn

© 2018 Chinese Physical Society and IOP Publishing Ltd

mainly on the equipment built in the State Key Laboratory of Electronic Thin Films and Integrated Devices which is also an International Cooperation Base. In the main text of the paper, we highlight key experimental results of LPE-garnet films and the important physics and applications based on these films. Given the huge volume of work which has been done over last 50 years since the first garnet film was fabricated by LPE, only several kinds of magnetic garnet films and devices will be discussed in this paper.

2. LPE equipment (vertical dipping technique)

2.1. Equipment

Liquid phase epitaxial garnet layers are grown on non-magnetic garnet substrates by using a horizontal dipping technique. Figure 1(a) shows a typical vertical dipping apparatus with a furnace, electronics for control and a computer for analyzing and observing the interactions. The accessories of the equipment, including a 100-mm diameter platinum alloy crucible, 1-inch (1 inch = 2.54 cm) and 3-inch subtract platinum alloy holder, and a platinum alloy stirrer as shown in Fig. 1(b). The temperature distribution within the furnace is measured and controlled by thermocouples and a proportional integral derivative (PID) system, which is connected to a control and display computer. The growth part of the equipment consists of a vertical five-zone furnace, a scavenging duct to extract fumes, mechanisms to handle substrate crystals, six fixed thermocouples, and a crucible table in the furnace. The five-zone furnace is shown in Fig. 1(c), the upper motor is for rotating the substrate while growing; the crucible table is for lifting the crucible into the furnace and locating it at the uniform temperature zone; the thermocouples is for measuring the temperatures of the five-zone in the furnace and the temperature of the crucible. The five-zone crucible consists of five separated heater coils. Since the furnace is an unsealed chamber, the upper heater and the lower heater insulate the internal and the external environment temperature. The inner three heaters are for controlling and stabilizing the temperature at the crucible position. The fluxed melts are contained by the crucible at high temperature (800 °C–1100 °C). Usually, we melt the oxides at a temperature of 100 °C higher than the undercooling temperature and stir for 12 h to fully melt the flux. Non-magnetic $Gd_3Ga_5O_{12}$ (GGG) and substituted GGG, e.g., Ca, Zr, Mg-doped GGG wafers are used as substrate crystals, and the diameter of a substrate is 75 mm. Single or multiple substrates are sustained by a jig made of platinum or platinum alloy. The GGG and substituted GGG wafers are prepared using the Czochralski method (crystal pulling) and sliced and polished. Liquid phase epitaxial garnet films grow on the substrates by dipping substrates into the slightly undercooled flux melts. By rotating substrates at a rotation speed of 50 rpm–100 rpm, garnet films of uniform thickness are obtained. After the growth of LPE films, substrates are withdrawn from the melt, and residual fluxed melts are removed by rotating the wafers at high speed. For Bi-substituted garnet films, however, the residual melt tends to adhere to the melt surface due to wetting, even after high-speed rotation. The surfaces of the Bi-substituted garnet films are stained with this residual fluxed melt. Since fluxed melt contains PbO and Bi_2O_3, with a relatively high vapour pressure at LPE temperature, fumes from these substances must be extracted through a scavenging duct, gathered and treated appropriately.

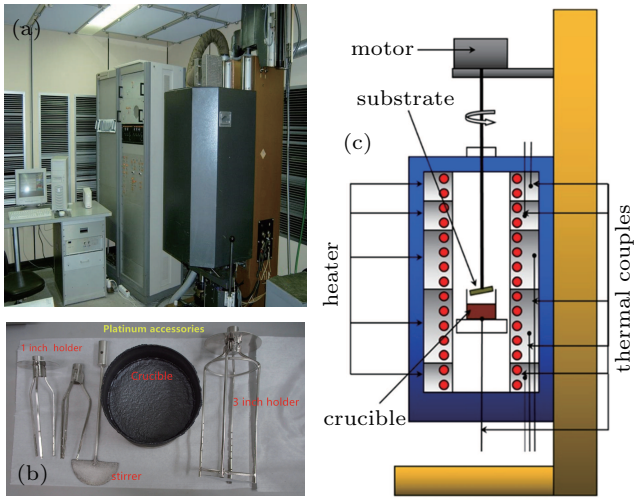


Fig. 1. (color online) (a) Photo of equipment, (b) platinum accessories, and (c) schematic diagram of the furnace.

2.2. Method

To grow single garnet crystals or single crystalline films, the knowledge of phase equilibria between the crystals and environment phases is indispensable. The phase relationship between Fe_2O_3 and $YFeO_3$ has been reported by van Hook;[4,5] $Y_3Fe_5O_{12}$ can be formed through a peritectic reaction between $YFeO_3$, which is a primary phase, and a melt, which contains more Fe_2O_3 than the $Y_3Fe_5O_{12}$ composition. Based on this phase diagram, highquality $Y_3Fe_5O_{12}$ single crystals were grown at temperatures between the peritectic (1555 °C) and eutectic (1469 °C) temperatures, either by a top-seeded solution growth or a travelling solvent-floating-zone method. Single crystal growth of $Y_3Fe_5O_{12}$ has been attempted for the first time from a PbO fluxed melt by Nielsen and Dearborn, i.e., a flux method. Through the flux growth of $Y_3Fe_5O_{12}$ single crystals, they prepared a phase diagram for the $PbO{\cdot}B_2O_3$–Y_2O_3–Fe_2O_3 system. Later, Jonker reported precise phase diagrams for the pseudo-ternary $PbO{\cdot}B_2O_3$–Y_2O_3–Fe_2O_3 system.[6] The solubility of rare earth oxides can

be enhanced by a factor of about ten if mixture of PbO–PbF_2 is used as solvent. The improvement in quality and size were obtained by adding a small amount of B_2O_3 into PbO and PbO–PbF_2. The PbF_2 has significant volatility and cannot be used in open crucible. Therefore, the current garnet films are grown by using solvent of PbO–B_2O_3–(Fe_2O_3) or PbO-Bi_2O_3–B_2O_3–(Fe_2O_3) for Bi-substituted magneto–optical garnets. For the LPE growth of Bi-substituted garnet cases, Bi ions acts both as solvent and as constituent.[7]

The base to understand the growth kinetics of any crystal in solution is the knowledge of the liquidus curve. Liquidus curves are mostly defined for pseudo-binary systems, consisting of solvent, e.g., PbO–B_2O_3–(Fe_2O_3) and solute, e.g., $Y_3Fe_5O_{12}$. Therefore, the phase transition liquid(l)–solid(s) is described for a so-called single-molecule model as

$$Y_3Fe5O_{12}(l) \leftrightarrow Y_3Fe5O_{12}(s),$$

where concentration is defined for a $Y_3Fe_5O_{12}$ molecule. Physico–chemical studies of different flux melts shows, however, that the garnets decompose into cation–oxygen complexes:

$$3YO_n^{3-2n} + 5FeO_m^{3-2m} \leftrightarrow Y_3Fe5O_{12}\,(s) + (3n + 5\,m - 12)O^{2-}(l),$$

where solubility products are defined for such species, which were comprehensively surveyed earlier.

3. Several kinds of magnetic garnet films

3.1. Yttrium iron garnet (YIG)

Yttrium iron garnet (YIG) is one of the most extensively studied magnetic materials with the smallest known magnetic relaxation parameter. Decades ago, the motivation was to apply micron or even thicker films of YIG to microwave devices, such as microwave delay line, filter, circulator, oscillator, etc. In 1988, several review papers gave a conclusion of about 30-year studies on YIG. After that, only a few articles concentrated on fabricating YIG films via new technology. The spin pumping effect in YIG/Pt structure invokes intensive studies of magnonic information transport and procession devices using single crystal YIG films. Unlike the previous study, the demand for submicron or nanometer devices requires the thickness of YIG films to be at the same as or smaller than that of the film with low damping coefficient and allows magnons to propagate over distances exceeding several centimetres. In this case, submicron YIG films aroused lots of interest.[8]

3.2. YIG thick films (1 μm–100 μm)

Due to the prolonged magnetic relaxation process in these materials, magneto-static surface and volume waves can propagate in the garnet film, allowing an analogue signal to be processed directly in the microwave range. Devices like filters, delay lines, oscillators and circulators have been designed by using such garnet films. These many devices need films with thickness more than few micrometres that cannot be obtained with pure YIG films grown on gadolinium gallium garnet (GGG) substrate without mechanical stresses and cracks induced by a lattice parameter mismatch of about 0.007 Å. In this case, we need to modify the lattice constant of YIG film without changing its magnetic properties. The garnet films with nominal composition $Y_{2.93}La_{0.07}Fe_5O_{12}$ were grown by the standard LPE method on a (111)-oriented GGG substrate from a supersaturated melt based on the PbO–B_2O_3 flux. The La:YIG thick films were thought to have the same magnetic properties as those of the YIG films. Using the found growth-strategy parameters, the La:YIG films with thickness up to 130 μm were successfully grown.[9] Figure 2(a) gives the scanning electron microscopy (SEM) image of La:YIG/GGG cross-section with an excellent interface. Figure 2(b) shows the perfect soft magnetic properties of La: YIG films with thickness up to 40 μm. Figure 2(c) gives the ferromagnetic resonance (FMR) spectrum of thick La:YIG film via magnetic hole method, the main peak shows a linewidth of 0.72 Oe (1 Oe = 79.5775 A·m^{-1}). Figure 2(d) displays the x-ray diffraction (XRD) spectrum of 44.41-μ m La:YIG film, the GGG peak and the La:YIG peak overlap, which means a perfect match between the substrate and the film.

Based on thick YIG films, many devices have been reported. In 1987, Yoshikazu *et al.*[10] used La:YIG (40 μm) to fabricate a tunable stripline band pass filter: when the bias field was between 1910 Oe and 3160 Oe, the centre frequency changed from 0.5 GHz to 4.0 GHz. To filter the low-frequency signal, the authors studied the response of YIG films with a crystal orientation of (111) and (100). The result showed that the frequency lower than 0.25 GHz cannot transmit in the (111) YIG film. In 2013, Yang *et al.* used local magnetisation technic to realize small tunable bias magnetic field YIG filter. The zero field centre frequency was about 6.17 GHz and 100 Oe bias field could tune about 320 MHz.[11] Ustinov *et al.* used YIG thin film to design an HSEW phase shifter, and according to the operation of the electric field and magnetic field they achieved a 5-GHz phase shifter, providing a reference for the spin wave application.[12] In 2015, Elena Bankowski *et al.* calculated and simulated the delay line with YIG films, and proposed the method to improve the delay of YIG.[13] Other devices like microwave circulator,[14–16] oscillator[17–20] were also proposed.

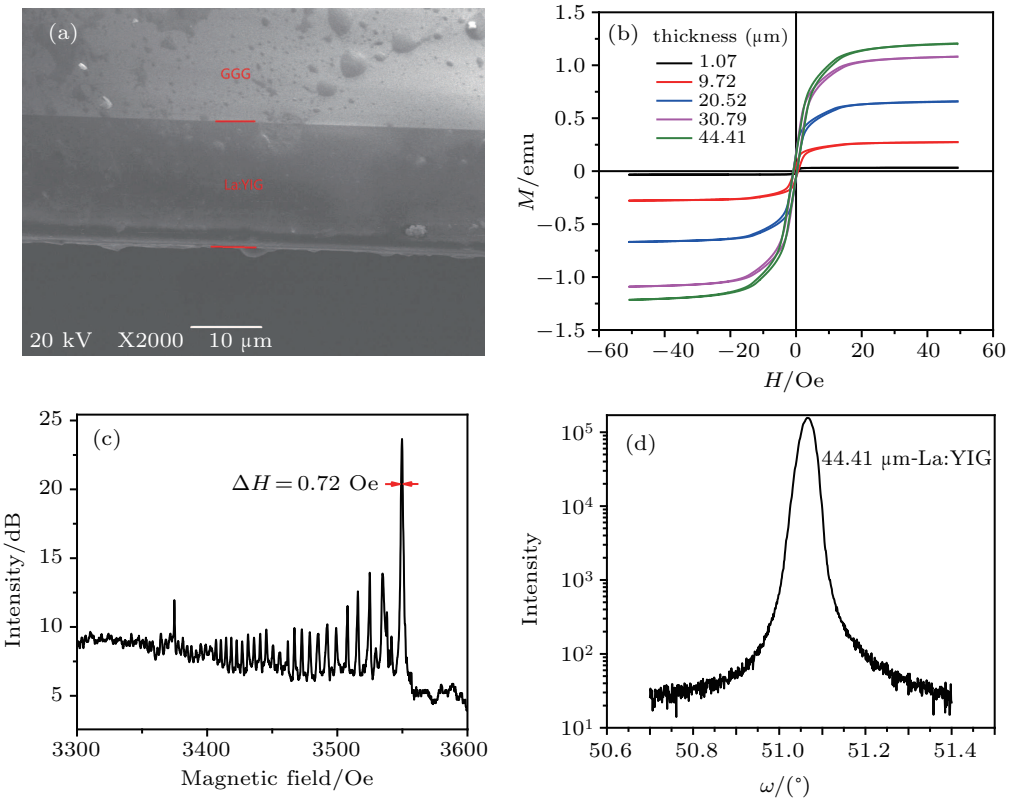


Fig. 2. (color online) (a) scanning electron microscopy (SEM) image of La:YIG/GGG cross-section, (b) magnetic hysteresis loops of La:YIG films, (c) FMR spectrum of thick La:YIG film, and (d) XRD spectrum of 44.41-μm La:YIG film.

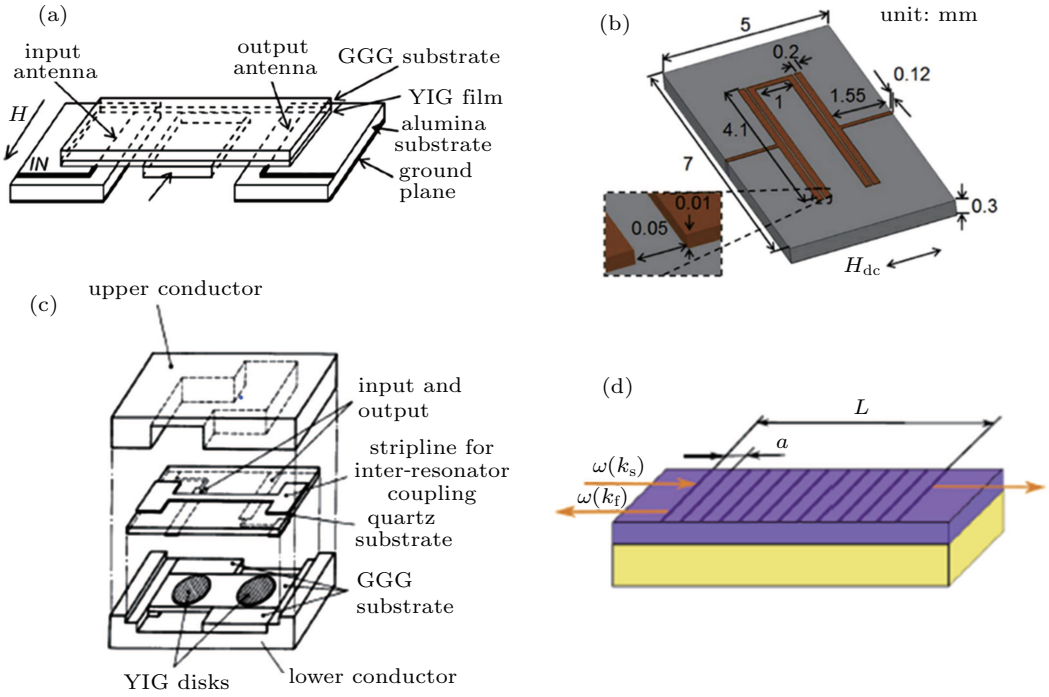


Fig. 3. (color online) microwave devices preparing YIG films for ((a) and (b)) tunable microwave filter,[12,21] (c) microwave phase shifter,[22] (d) microwave delay line.[13]

3.3. YIG thin films (0.1 μm–1 μm)

The main techniques for growing YIG films are LPE for thick films (1 μm to 100 μm) and RF sputtering or PLD for thin films (< 100 nm). One is trying to reduce the thickness to the nanoscale by using LPE to obtain YIG thin films with lower damping than those fabricated by RF sputtering or PLD. With a few years' development, YIG films thinner than 200 nm have been produced by LPE and have been used in some areas. However, LPE fabricated YIG films with thickness larger than 1 μm[23] and smaller than 100 nm have quite different magnetic properties.[2] To obtain nanoscale YIG thin films via

LPE, several technological conditions should be carefully controlled. The first one is the Blank- Nielsen ratio, and a lower concentration can help reduce the growth rate. The second one is to control the growth temperature, making it as high as possible under the condition without significantly increasing the impurity (Pb^{2+}, Pb^{4+}, Pt^{4+}) density in the film, and to control the rotation rate, transfer rate, etc.

The YIG (444) and GGG (444) peaks were mostly overlapped due to the tiny lattice mismatch. As the YIG film thickness increased, the right shoulders of the curves increased in intensity, which means a tensile-stressed YIG film. In contrast, the XRD peak in La: YIG film showed almost no shoulder on either side of the GGG peak and a smaller linewidth than that of GGG/YIG, indicated by the red curve in Fig. 4(a). The comparing HRXRD results give evidence of existence of tensile stress for pure YIG film epitaxially grown on GGG. The YIG film fabricated by RF sputtering or PLD on a GGG substrate showed a YIG diffraction peak with a lower Bragg angle than that on the GGG substrate, indicating considerable distortion of the YIG garnet cell.[24–27] Figure 4(b) compares the magnetic hysteresis loops of YIG and La:YIG films with approximately equal thickness, revealing three phenomena that should be mentioned. First, at low film thickness (110 nm) the YIG film has a better magnetic hysteresis loop squareness ratio than the La:YIG film. Second, the magnetic hysteresis loops of the YIG film shows a thickness dependence, while those of the La:YIG films are stable across all studied thickness. Third, the 1000-nm-thick YIG film showeds relatively high H_c and H_s, while the La:YIG film still exhibits low H_c and H_s. The facts above show the essential difference between the GGG/YIG and GGG/La:YIG structures. Our La:YIG films were considered to be $La_{0.07}Y_{2.93}Fe_5O_{13}$. The La^{3+} replaced part of the Y^{3+} at the dodecahedron site, distorting the sublattices and further increasing the lattice parameter. This increase in lattice parameter leads to a perfect match with the GGG substrate as shown in the film prepared by HRXRD. In this case, the GGG/La:YIG interface has almost no stress, which is why the magnetic hysteresis loop is not thickness dependent. The lattice distortion affects both the tetrahedral site and the octahedral site, which is occupied by the antiparallel magnetic moment of Fe^{3+}. The thickness of the easy magnetization area is can be estimated at about 423 nm, and the stress relaxation seems to start from this thickness.

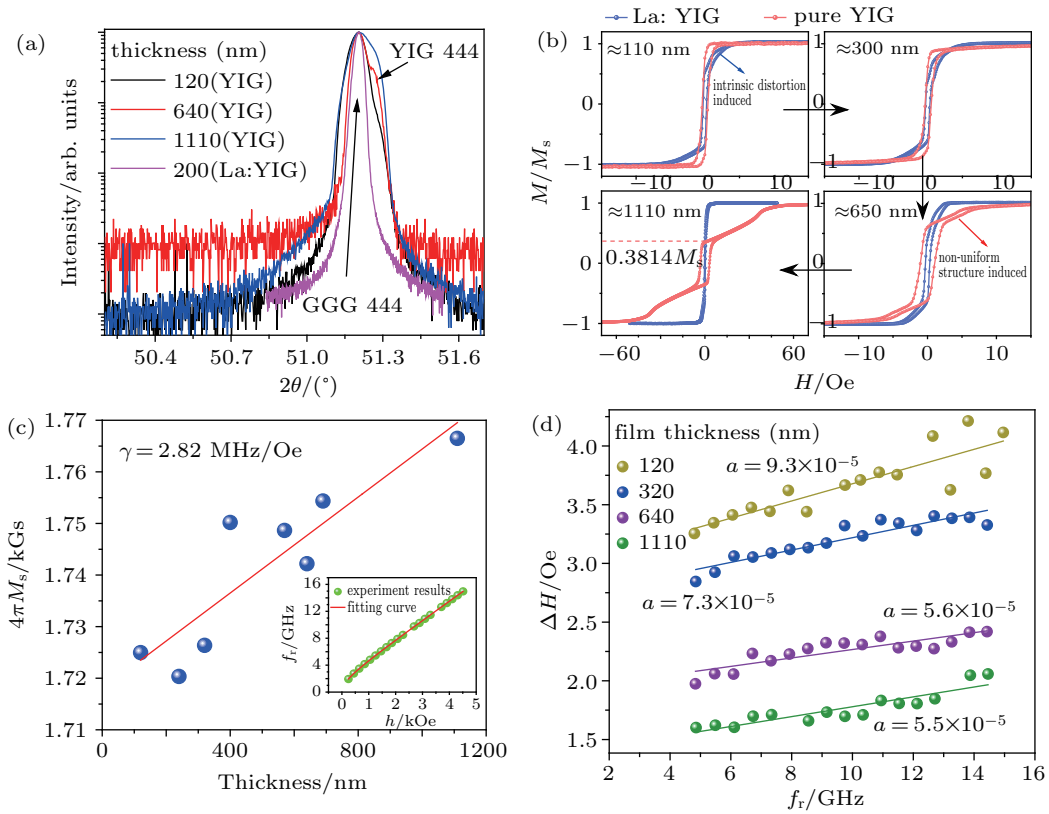


Fig. 4. (color online) (a) HRXRD, ω-scan near the 444 Bragg reflection of the substrate/film; (b) magnetic hysteresis loops of YIG and La:YIG at various thickness; (c,) $4\pi M_{\rm eff}$ abstracted from FMR measurement as a function of film thickness; (d) frequency dependence of the FMR linewidth for YIG LPE films with various thickness. The unit 1 Gs = 10^{-4}T.

The $4\pi M_{\rm eff}$ values shown in Fig. 4(c) are fit from FMR results by using the Kittel formula

$$\pi f_{\rm r} = (\gamma\mu_0/2\pi)\sqrt{H(H+4M_{\rm eff})},$$

where $f_{\rm r}$ is the resonant frequency at the fixed magnetic field H applied during the measurement, and $\gamma/2\pi = 2.82$ MHz/Oe is the gyromagnetic ratio.[28] As shown in Fig. 4(c), $4\pi M_{\rm eff}$

increases with film thickness increasing. The first reason is the stress-induced nonuniform region causing the two-magnon scattering[29,30] as shown in the measured M–H loops. The YIG lattice at the GGG/YIG interface follows the lattice of GGG, increasing the lattice and an effective positive field of uniaxial and magneto-crystalline anisotropy, which are usually observed in a YIG film.[31] The fit lines in Fig. 4(d) show the damping of film with thickness increasing. The 120-nm-thick YIG film shows the damping of 9.3×10^{-5}, which is a rather good result for a YIG thin film. The extracted Gilbert damping parameter for the 1110-nm-thick YIG film is as low as 5.5×10^{-5}.

The cutting-edge research of YIG film is called YIG magnonics[32] or magnon spintronics.[33] Historically, bulk YIG crystals were used for studying magnonics on a micrometertomillimeter length scale needed for microwave devices. However, fabrication of integrated spintronic, magnonics or magneto–optical devices requires thin films with high structural and magnetic quality, instead. In particular, achieving very low damping in thin film YIG is a critical factor for fabricating the magnonics logic devices to transport, store, and process microwave and digital information for the post-CMOS (where CMOS stands for complementary metal–oxide–semiconductor) era. Applications include integrated multi-modal spin-wave devices, delay lines, filters, resonators, generators, multi-channel receivers, directional couplers, and Y-junctions. Also, low damping can be utilized for spin-based resonant sensing applications.[34–36] Here we introduce four most studied devices or structures.

The seminal letter to Kajiwara *et al.* in 2010, showed that by depositing platinum strip (Pt, a normal metal) on the top of a 1.3-μm-thick yttrium iron garnet (a magnetic insulator), one could efficiently transfer spin angular momentum through the interface and generate voltage via inverse spin Hall effect in Pt as shown in Fig. 5(a). This finding was followed by comprehensive studies of this phenomenon: the dependence on the thickness of the non-magnetic metal and the YIG layer, as well as on the applied microwave power has been reported. The influence of the interface condition on the spin-pumping efficiency was revealed, and the contributions to the SP effect by different spin-wave modes were studied.[37–42]

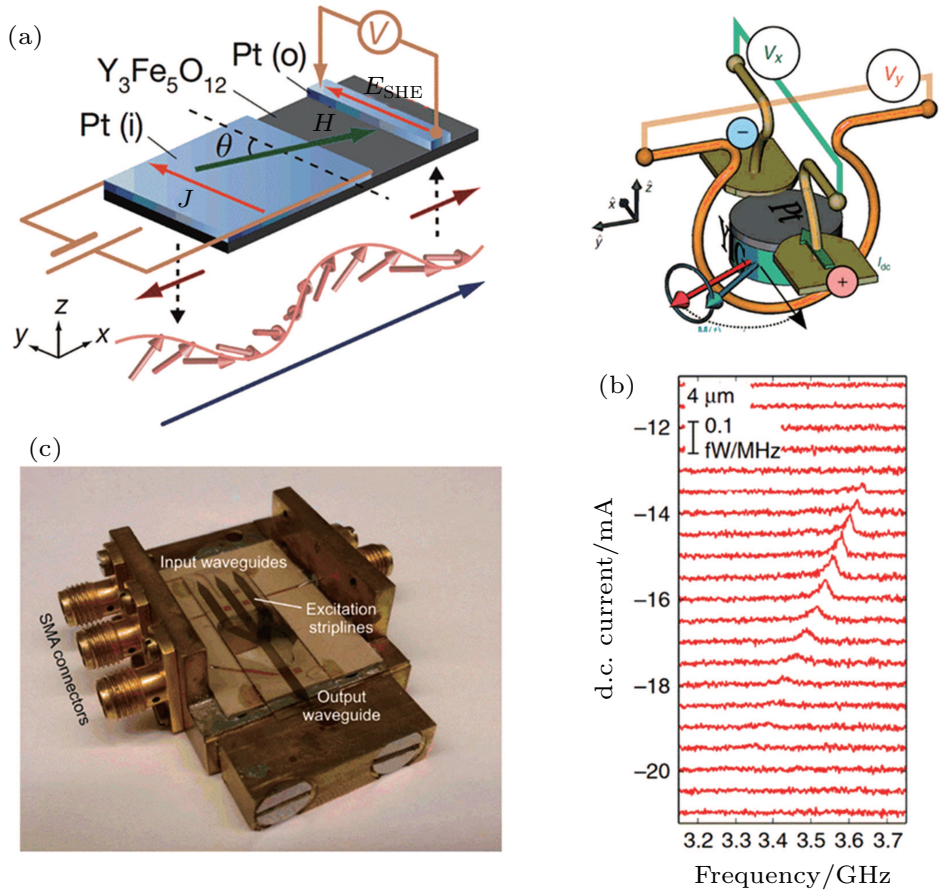


Fig. 5. (color online) Prototype devices of (a) electric-signal transmission via spin-wave spin currents by Kajiwara *et al.*,[37] (b) spin-torque nano-oscillator (STNO) by Collet *et al.*,[43] and (c) spin wave logic device or spin-wave majority gate by Fischer *et al.*[44]

To combine magnonic devices with electronic circuits, efficient means for magnon excitation by a charge current are required. Although magnons can be injected relatively easily by an a.c. electric current (for example, using antenna structures), it is a complicated problem if a d.c. current is used. One of the most promising solutions is to use the spin-transfer-torque

(STT) effect. In 2016, Collet, *et al.* first reported the direct electrical detection of auto-oscillation in YIG/Pt structure and showed that the threshold current is increased by the presence of quasi-degenerate SW modes.[43] This implies that the careful engineering of the spin-wave mode spectrum is required to optimize magnonic devices by making use of spin-orbit effect as shown in Fig. 5(b).

The scaling of conventional CMOS-based nanoelectronics is expected to become increasingly intrinsically limited in the next decade. Therefore, novel beyond-CMOS devices are being actively developed as a complement to expand functionally in future nanoelectronics technology nodes. In particular, the field of magnonics, which utilizes the fundamental excitations, i.e., spin waves and their quanta, of a magnetic system,magnons, as data carriers to provide the promising approaches to overcomeing crucial limitations of CMOS since they may provide ultralow power operation and nonvolatility. This report demonstrated the experimental realization of a majority gate based on the interference of spin waves as shown in Fig. 5(c). Here, the phase of the output signal is defined by the majority of the phases of the input signals. Recent progress of the miniaturization of YIG structures and techniques for a phase control by electric currents, by electric fields as described in the work by Ustinov *et al.*, or by spin-polarized currents, and by a combination of domain wall-based waveguides and dot arrays, provides the promising drafts for the required advances towards applications.[44]

3.4. Magneto–optical garnet films

Progress of integrated optics relies heavily on the development of single-crystal films which can serve both as optical waveguides and as active medium in electro- or magneto–optical devices. The single-crystal epitaxial garnet films on nonmagnetic garnet substrates can be used as optical waveguide at visible and infrared wavelengths. The use of garnet films as optical waveguides was first discussed. Films like these were developed for magnetic bubble devices, and some of them are found to have magnetic properties useful in integrated optics. In fact, Tien *et al.*[45] have constructed a novel magneto–optical switch using a scandium-substituted yttrium iron garnet film, in which the light wave in one of the waveguide modes can be switched on and off by a small magnetizing circuit. The details of this magneto–optical switch and other magnetic film devices will be discussed elsewhere.[46,47]

3.5. Growth and magneto–optical properties of large sized single-crystal thick TmBiIG films from lead-free Fflux by LPE technology

Bismuth substituted iron garnet films have been shown to be a prospective material for magneto–optic (MO) device applications such as Faraday isolators, MO modulators, visualizers, magneto-static wave devices, etc.

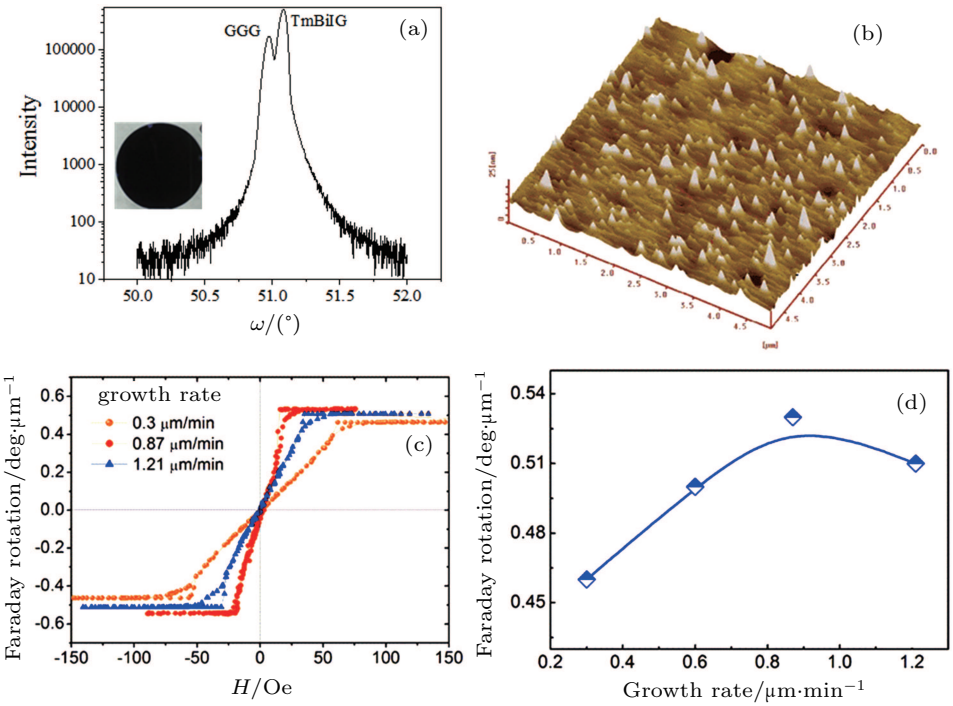


Fig. 6. (color online) (a) XRD spectrum of 3-inch epitaxy Bi:TmIG thick film, (b) AFM image of epitaxy film, (c) NanoMOKE measurement of Bi:TmIG films with different growth rates, and (d) Faraday rotation as a function of growth rate.

The garnet films of nominal composition $Tm_{2.28}Bi_{0.72}Fe_{4.3}Ga_{0.7}O_{12}$ were grown by standard LPE method on (111)-oriented GGG substrates each with a 3-inch diameter from a supersaturated melt based on the Bi_2O_3 flux. To calculate a charge composition the mole ratios (Blank–Nielsen coefficients) were used as follows:

$$R_1 = \frac{Tm_2O_3}{Fe_2O_3} + Ga_2O_3 = 0.1 - 0.2;$$
$$R_2 = \frac{Ga_2O_3}{Fe_2O_3} = 0.1 - 0.135;$$
$$R_2 = \frac{B_2O_3}{Bi_2O_3} = 0 - 0.064;$$
$$R_4 = \frac{\text{Garnet}}{\text{Garnet} + \text{Flux}} = 0.1 - 0.2.$$

After growth process the film surface is covered with flux residuals due to the high viscosity and adhesion of Bi_2O_3 based flux. To avoid the complicated high-speed rotation procedure to spin off the flux residuals, the film was kept after growth process above melt during some time till the full cleaning of film surface.[48,49] The Bi:TmIG films of thickness 50 μm–60 μm were obtained using growth rates between 0.8 μm/min and 0.9 μm/min. The mismatch between the film and the GGG substrate is nearly completely mitigated. The FRA reached its maximum value of 0.54 μm/min, which is due to the slight increase in the number of Bi^{3+} ions in the film composition and leads to the splitting of excited energy levels. The combination of large size, excellent MO, and soft magnetic properties of these films leads to a wide scale adoption in MO and integrated magnetic devices.

3.6. Magneto–optical and microwave properties of LuBiIG thin films prepared by LPE method from lead-free flux

Recently, integrated circuits with both MO and microwave devices have rapidly developed, and a new kind of garnet film combining good optical, MO effect and proper microwave properties are urgently needed. The $(Bi:Lu)_3Fe_5O_{12}$(LuBiIG) film is a kind of film that can meet these requirements, and it can be used in MO and microwave hybrid integrated systems. On the other hand, the fluxes used to grow garnet film by the LPE method are $PbO–B_2O_3(–Bi_2O_3)$, $BaO–BaF_2–B_2O_3$, and $MoO_3–Li_2O$ fluxes.[50] Of them, $PbO–B_2O_3(–Bi_2O_3)$flux is most commonly used because it provides high growth rate and low growth temperature. However, the PbO flux is mordant and poisonous. Moreover, Pb ions would be incorporated into the garnet films in the epitaxy process, which has a seriously negative influence on the performances of microwave devices, both the optical and magneto–optical properties. Therefore, the growth of films from PbO-free flux is crucial to improving the quality and properties of YIG films. Non-magnetic Bi^{3+} ions and Lu^{3+} ions were incorporated into the garnet matrix to obtain large MO effect, and thus improving the lattice match between the film and the GGG substrate, respectively. In this paper, by optimizing the growth conditions, high-quality garnet films were successfully fabricated on GGG (111) substrates by the LPE method with Bi_2O_3 as the melting agent. The crystal structure, microwave characteristic and magnetic properties, as well as the optical and MO properties are investigated. An FMR linewidth of $2\Delta = 2.8$ Oe–5.1 Oe and a Faraday rotation of 1.64 deg/μm at 633 nm are obtained. Our film is a very attractive material for applications in microwave and MO as shown in Fig. 7.

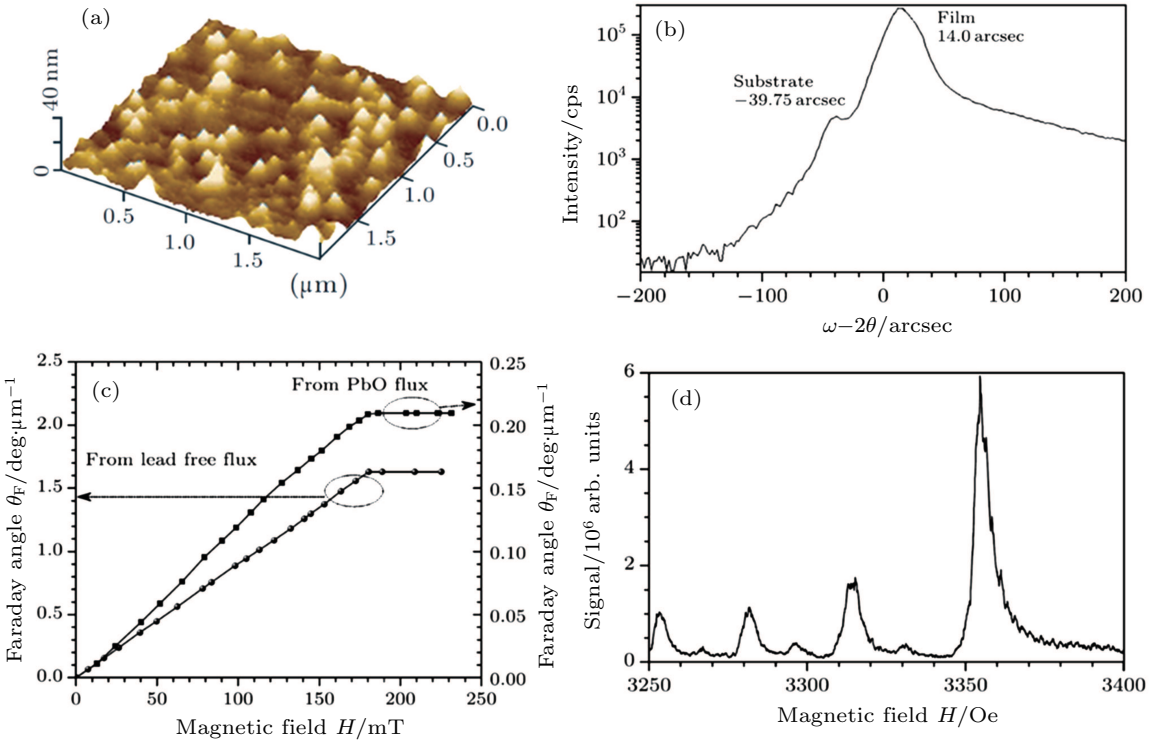


Fig. 7. (color online) (a) The AFM image of the surface pattern of the LuBiIG thin film, (b) the XRD pattern of LuBiIG thin film on GGG substrate, (c) the FMR spectra versus ΔH of LuBiIG film on GGG substrate, and (d) specific Faraday rotation θ_F versus external magnetic field at 633 nm at room temperature.

We also investigate the absorption coefficients of LuBiIG thin film from microwave band to optical band. In microwave band, the absorption coefficient is represented by FMR linewidth and a very small value of $2\Delta H = 2.8$ Oe–5.1 Oe is obtained. In optical band, the absorption coefficient is as low as 600 cm^{-1} in the visible range. In THz band, very low absorption coefficient is obtained to be less than 0.3 cm^{-1} in a frequency range of 0.37 THz–0.95 THz and the minimum value 0.05 is observed at 2.24 THz. The combination of good optical, microwave, and THz properties of this garnet film indicates wide applications, such as in optical devices, magnetostatics wave devices, THz wave guide, and some integrated devices or systems.

Here, we list some of MO films which have not been motioned above. Due to the wide range of dopants available for garnet, lots of research work has been done to find the best MO materials, including $Y_3Ga_{1.1}Sc_{0.4}Fe_{3.5}O_{12}$ with $4\pi M_s$ of 600 Gs with an optical rotation of 0.0208 deg/μm,[45] the $Gd_{3-x}Bi_xFe_5O_{12}$ film with an optical rotation of 2.38 deg/μm,[51] the LuSmIG film with an optical rotation of 2 deg/μm,[52] the $(LuNdBi)_3(FeA1)_5O_{12}$ film,[53] the $Y_{1.43}Yb_{0.82}Bi_{0.75}Fe_5O_{12}$ film,[54] and $(Bi, Lu)_3(Fe, Ga)_5O_{12}$ film.[55]

3.7. Magneto–optical devices

Magnetic garnets have a number of unusual properties which make them attractive for applications in devices. Due to the three magnetic sublattices which are ferrimagnetically coupled, magnetic garnets have a unique magneto–optical property: no any other magnetic material can rotate the polarization plane of light by the Faraday effect in a spectral region where the optical absorption is zero. The heat treatment and doping can considerably change the electrical properties of garnet film by as great as eight orders.[56] A number of magneto–optical devices have been conceived and designed, and several working prototypes were built in the 1970 s. Figure 8 shows for the first time switching and modulation of light in a magneto–optic waveguide that is a single-crystal epitaxially grown iron-garnet film. These experiments involve the Faraday rotation of the magnetic film and the motion of magnetization in the plane of the film. We have modulated light from a 1.152-μm laser up to 80 MHz. We were also able to switch light between two waveguide modes by applying a magnetic field as small as 0.2 Oe. Figure 9 shows a waveguide optical isolator employing a nonreciprocal phase shift.[53] The isolator has the advantage of needing neither phase-matching nor complicated magnetization control. It is shown that the degradation of characteristics due to deviations in the waveguide parameters can be retained within an acceptable limit by current technologies. Also, a rare earth iron garnet crystal suitable for constructing this isolator has been developed. Magnetostatic backward volume wave (MSBVW) efficiently enters into the film as expected from the measured small ferromagnetic resonance linewidth of 0.7 Oe, whereas magnetostatic surface wave and magnetostatic forward volume wave are subjected to the severe attenuation due to their coupling to spin-wave modes. The interaction between guided optical wave and MSBVW is investigated in a transverse configuration where the input optical wave passes almost orthogonally to MSBVW. The TM–TE optical-mode conversion induced by MSBVW is observed in a frequency range of 3.5 GHz–7.5 GHz. The experimental setup is shown in Fig. 10. Its efficiency, as high as 47%/0.8 W at 4 GHz, is obtained for the interaction length of 7 mm.[57]

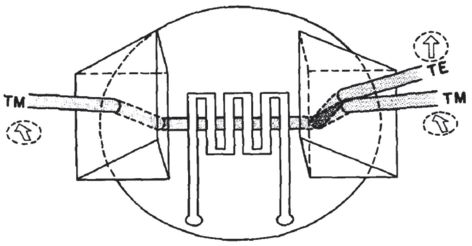
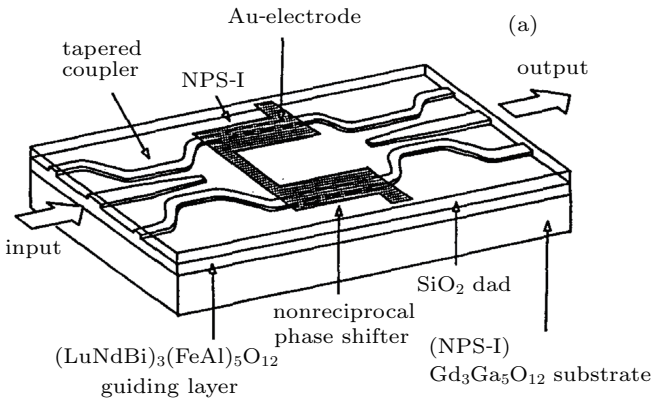


Fig. 8. Experimental arrangement of magneto–optical guided-wave modulator proposed by Tien *et al.*[45]



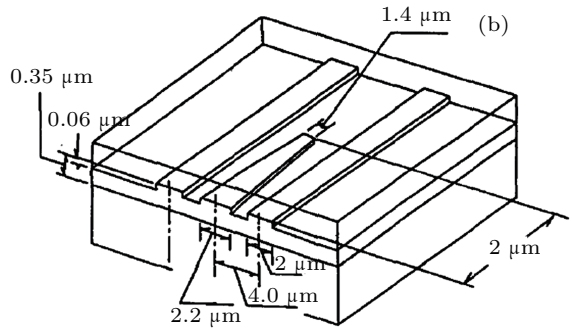


Fig. 9. (a) Structure of interferometric waveguide isolator employing nonreciprocal phase shift, and (b) branching device composed of tapered coupled waveguides by Mizumoto *et al.*[53]

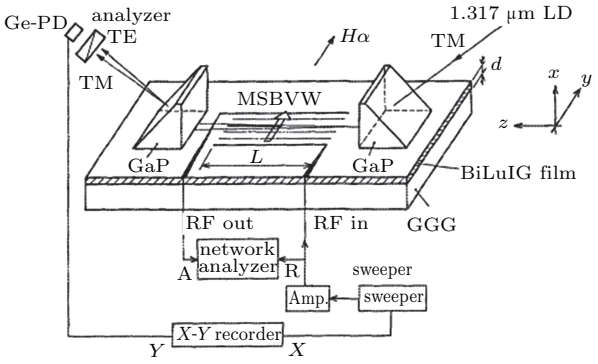


Fig. 10. Experimental setup for TM–TE mode conversion induced by MSBVW by Tamada *et al.*[57]

4. Conclusions

In this paper, we have reviewed the vertical dipping technique of LPE equipment built in the State Key Laboratory of Electronic Thin Films and Integrated Devices. We focus on several most studied magnetic garnet single crystal films, which have applications in the fields of microwave devices, magnetic and magneto–optical devices. We discuss the fabrication and applications of the pure $Y_3Fe_5O_{12}$ thin film, the $Y_{2.93}La_{0.07}Fe_5O_{12}$ thick film, the $(Bi, Lu)_3Fe_5O_{12}$ film, and the $Tm_{2.28}Bi_{0.72}Fe_{4.3}Ga_{0.7}O_{12}$ film. Our main aim is to try to combine the highquality magnetic garnet films with the urgent applications and the cutting-edge researches. Furthermore, we want to break the old concepts of LPE as an unstable technology, a method for thick films and a polluting method (PbO).

References

[1] Capper P and Mauk M 2007 *Liquid phase epitaxy of electronic, optical and optoelectronic materials* Vol. 21 (John Wiley & Sons) pp. 1–6
[2] Dubs C, Surzhenko O, Linke R, Danilewsky A, Bruckner U and Dellith J 2017 *J. Phys. D: Appl. Phys.* **50** 204005
[3] Liu Y, Wang X, Zhu J, Huang R S and Tang D M 2017 *Chin. Phys. B* **26** 057501
[4] Hook H 1961 *J. Am. Ceram. Soc.* **44** 208
[5] Kestigian M 1967 *J. Am. Ceram. Soc.* **50** 165
[6] Kimura S and Shindo I 1977 *J. Cryst. Growth* **41** 192
[7] Nielsen J and Dearborn E 1958 *J. Phys. Chem. Solids* **5** 202
[8] Kang Y, Zhong H, Hao R R, Hu S J, Kang S S, Liu G L, Zhang Y, Wang X R, Yan S S, Wu Y, Yu S Y, Han G B, Jiang Y and Mei L M 2017 *Chin. Phys. B* **26** 047202
[9] Syvorotka I I, Syvorotka I M and Ubizskii S B 2013 *Solid State Phenomen* **200** 250
[10] Murakami Y, Ohgihara T and Okamoto T 1987 *IEEE Trans. Microwave Theor. Techniq.* **35** 1192
[11] Yang X, Wu J, Beguhn S, Nan T, Gao Y, Zhou Z and Sun N X 2013 *IEEE Microwave Wireless Components Lett.* **23** 184
[12] Ustinov A B, Kalinikos B A and Srinivasan G 2014 *Appl. Phys. Lett.* **104** 052911
[13] Bankowski E, Meitzler T, Khymyn R S, Tiberkevich V S, Slavin A N and Tang H X 2015 *Appl. Phys. Lett.* **107** 122409
[14] Rahmouna E B and Faouzi S B 2013 *IJIEEE* 3
[15] Samad B A 2010 *J. Electromag. Waves Appl.* **3** 1123
[16] Zahwe O, Sauviac B and Rousseau J J 2009 *Prog. Electromag. Res.* **8** 35
[17] Zhang D S, Song W J and Chai G Z 2017 *J. Phys. D: Appl. Phys.* **50** 205003
[18] Ustinov A B, Nikitin A A and Kalinikos B A 2015 *IEEE Magn. Lett.* **6** 1
[19] Ustinov A B, Nikitin A A and Kalinikos B A 2015 *Tech. Phys.* **60** 1392
[20] Marcelli R, Andreta E, Bartolucci G, Cicolani M and Frattini A 2000 *IEEE Trans. Magn.* **36** 3488
[21] Sweet A A and Parrott R 2014 *Wireless and Microwave Technology Conference (WAMICON)*, 2014 IEEE 15th Annual, pp. 1–3
[22] Murakami Y, Ohgihara T and Okamoto T 1987 *IEEE Trans. Microwave Theor. Techniq.* **35** 1192
[23] Syvorotka I I, Syvorotka I M and Kityk I V 2010 *J. Magn. Mag. Mater.* **322** 3314
[24] Krysztofik A, Coy L E, Kuswik P, Zaleski K, Glowinski H and Dubowik J 2017 *Appl. Phys. Lett.* **111** 192404
[25] Howe B M, Emori S, Jeon H M, Oxholm T M, Jones J G, Mahalingam K, Zhuang Y, Sun N X and Brown G J 2015 *IEEE Magn. Lett.* **6** 1
[26] Onbasli M C, Kehlberger A, Kim D H, Jakob G, Klaui M, Chumak A V, Hillebrands B and Ross C A 2014 *APL Mater.* **2** 106102
[27] Liu T, Chang H C, Vlaminck V, Sun Y Y, Kabatek M, Hoffmann A, Deng L J and Wu M Z 2014 *J. Appl. Phys.* **115** 17A501
[28] Kalarickal S S, Krivosik P, Wu M Z, Patton C E, Schneider M L, Kabos P, Silva T J and Nibarger J P 2006 *J. Appl. Phys.* **99** 093909
[29] Jermain C L, Paik H, Aradhya S V, Buhrman R A, Schlom D G and Ralph D C 2016 *Appl. Phys. Lett.* **109** 192408
[30] Landeros P, Arias R E and Mills D L 2008 *Phys. Rev. B* **77** 214405
[31] Manuilov S A and Grishin A M 2010 *J. Appl. Phys.* **108** 013902
[32] Serga A A, Chumak A V and Hillebrands B 2010 *J. Phys. D: Appl. Phys.* **43** 264002
[33] Chumak A V, Vasyuchka V I, Serga A A and Hillebrands B 2015 *Nat. Phys.* **11** 453
[34] Ishak W S 1988 *Proc. IEEE* **76** 171
[35] Bernstein K, Cavin R K, Porod W, Seabaugh A and Welser J 2010 *Proc. IEEE* **98** 2169
[36] Maze J, Stanwix P, Hodges J, Hong S, Taylor J, Cappellaro P, Jiang L, Dutt M G, Togan E and Zibrov A 2008 *Nature* **455** 644
[37] Kajiwara Y, Harii K, Takahashi S, Ohe J, Uchida K, Mizuguchi M, Umezawa H, Kawai H, Ando K, Takanashi K, Maekawa S and Saitoh E 2010 *Nature* **464** 262
[38] Ando K and Saitoh E 2012 *Phys. Rev. Lett.* **109** 026602
[39] Kurebayashi H, Dzyapko O, Demidov V E, Fang D, Ferguson A J and Demokritov S O 2011 *Nat. Mater.* **10** 660
[40] Qu D, Huang S Y, Hu J, Wu R and Chien C L 2013 *Phys. Rev. Lett.* **110** 067206
[41] Jungfleisch M B, Chumak A V, Kehlberger A, Lauer V, Kim D H, Onbasli M C, Ross C A, Kläui M and Hillebrands B 2015 *Phys. Rev. B* **91** 134407
[42] Mendes J B S, Cunha R O, Alves Santos O, Ribeiro P R T, Machado F L A, Rodríguez-Suárez R L, Azevedo A and Rezende S M 2014 *Phys. Rev. B* **89** 140406
[43] Collet M, de Milly X, d'Allivy Kelly O, Naletov V V, Bernard R, Bortolotti P, Ben Youssef J, Demidov V E, Demokritov S O, Prieto J L, Munoz M, Cros V, Anane A, de Loubens G and Klein O 2016 *Nat. Commun.* **7** 10377
[44] Fischer T, Kewenig M, Bozhko D A, Serga A A, Syvorotka I I, Ciubotaru F, Adelmann C, Hillebrands B and Chumak A V 2017 *Appl. Phys. Lett.* **110** 152401
[45] Tien P, Martin R, Wolfe R, Le Craw R and Blank S 1972 *Appl. Phys. Lett.* **21** 394
[46] Yang G, Zhang G Y, Gao J, Xue L P, Xia T and Zhang X L 2011 *Chin. Phys. B* **20** 017802
[47] Liang H, Liu H, Zhang Q, Fu S F, Zhou S and Wang X Z 2015 *Chin. Phys. B* **24** 67807
[48] Syvorotka I, Syvorotka I, Ubizskii S, Kumar P and Prabhakar A 2014 *IEEE International Conference on Oxide Materials for Electronic Engineering (OMEE)* pp. 201–202
[49] Zhang D, Mei B, Zhang H, Yang Q and Rao Y 2015 *IEEE Trans. Magn.* **51** 1
[50] Korenstein R and Castro C A 1979 *J. Appl. Phys.* **50** 7830
[51] Hansen P, Witter K and Tolksdorf W 1983 *Phys. Rev. B* **27** 4375
[52] Mada J and Yamaguchi K 1985 *J. Appl. Phys.* **57** 3882
[53] Mizumoto T, Mashimo S, Ida T and Naito H 1993 *IEEE Trans. Magn.* **29** 3417
[54] Tepper T, Ilievski F, Ross C A, Zaman T R, Ram R J, Sung S Y and Stadler B J H 2003 *J. Appl. Phys.* **93** 6948
[55] Iida K, Kawamae N, Hoshi S, Machi T, Kono T, Yoshioka-Kato J, Chikumoto N, Koshizuka N, Adachi N and Okuda T 2005 *Jpn. J. Appl. Phys.* **44** 1734
[56] Paroli P 1984 *Thin Solid Films* **114** 187
[57] Tamada H, Kaneko M and Okamoto T 1988 *J. Appl. Phys.* **64** 554